Two Dimensional Simulation of Film Boiling Heat Transfer in Complex Geometries Using Front Tracking Method

A.Sedaghatkish, S.Mortazavi*

Isfahan University of Technology, Isfahan, Iran

ABSTRACT: Film boiling has various industrial applications, especially in heat exchangers. Studying this phenomenon on complex geometries and investigating heat transfer coefficient is desired by many industries. The numerical method used here is a finite difference/ front tracking method which is developed independently for film boiling in complex geometries. The film boiling over two or more cylinders is simulated using this method. The effects of spacing, angle, and diameter are investigated for two cylinders. For the case with many cylinders, the effects of different geometrical configurations (regular and staggered) and the number of rows are investigated by calculating the average Nusselt number on each cylinder. It is observed that the cylinder spacing does not have any significant effect on the Nusselt number for the upper cylinder. However, the angle and cylinder diameter significantly affect the Nusselt number for the upper cylinder. In the regular configuration, the Nusselt numbers for the upper cylinders are relatively uniform and higher than lower cylinders. In the staggered configuration, however, the Nusselt numbers of the upper cylinders are different, non-uniform, and higher than those of the simple geometry.

1- Introduction

So far, many developments have been performed to improve heat transfer in chemical and oil industries as well as power plants. Researchers are still trying to maximize the heat transfer coefficient, which results in enhanced efficiency, reduced energy consumption, lower demand for construction materials, lower cost of fuel and optimization of the space required for constructing heat exchangers. In natural convection, single phase fluid flow occurs at a heat transfer coefficient in the range 5-10 W/m²K and 100-200 W/m²K for gases and liquids, respectively. In forced convection, the coefficient reaches 30-150 W/m²K and 100-1000 W/m²K for gases and liquids, respectively. For multiphase flows (e.g. boiling and condensation), however, heat transfer coefficient may reach as high as 4000-5000 W/m²K. Such a high heat transfer coefficient during the boiling process may resolve difficulties with respect to the heat transfer coefficient for designers of heat exchangers [1]. One of the most recent works performed in this respect is that by Kang [2]. In his experiments, he investigated the effect of two pipes and heat flux of every pipe on heat transfer coefficient. The evident effect of the two pipes in heat transfer coefficient is visible when heat flux of the lower pipe exceeds that of the upper one, and heat flux of the upper pipe being below 60 kW/m². The bubbles, rising from the surface of the pipes, were imaged at different flow conditions. When heat fluxes are low, larger bubbles are observed on the upper pipe. They found that the higher the heat fluxes, the larger will be the size of bubbles. The numerical method used here is a finite difference/ front tracking method which is developed independently for film boiling in complex geometries. Obtaining Nusselt number for different cylinders in staggered and simple arrangement

and predicting the shape of vapor layers rising from cylinders surface and how they interact with each other, are the most purposes of this research.

2- Methodology

All the governing equations for film boiling phenomenon are considered in this section. These include conservation of mass, momentum, and energy, and the source terms that enter the formulation. Furthermore, the boundary condition for a solid body such as a circular cylinder is explored in detail. In general, conservation equations (including mass, momentum, and energy) are written as follows (for details, please refer to Esmaeeli and Tryggvason [3]).

$$\frac{D\rho}{Dt} + \rho \nabla . \boldsymbol{u} = 0 \qquad (1)$$

$$\frac{\partial \rho \boldsymbol{u}}{\partial t} + \nabla . \rho \boldsymbol{u} \boldsymbol{u} = -\nabla P + \rho \boldsymbol{g}$$
$$+ \nabla . \mu (\nabla \boldsymbol{u} + \nabla \boldsymbol{u}^T) + \boldsymbol{f}_m \qquad (2)$$

$$\frac{\partial \rho c T}{\partial t} + \nabla . \rho c \boldsymbol{u} T = \nabla . k \nabla T + f_e \qquad (3)$$

Here, viscous dissipation term in the energy equation is neglected since the velocity gradient is small in the present problem. The above equations are valid in different phases, but the conditions for the jump at the interface for the mass and momentum and energy equations are defined as follows:

Corresponding author, E–mail: saeedm@cc.iut.ac.ir

$$\rho_l (\boldsymbol{u}_l - \boldsymbol{u}_f).\boldsymbol{n} = \rho_v (\boldsymbol{u}_v - \boldsymbol{u}_f).\boldsymbol{n} = \dot{m} \qquad (4)$$

$$\dot{m}(\boldsymbol{u}_v - \boldsymbol{u}_l) = (\tau_v - \tau_l).\boldsymbol{n} - (P_v - P_l)I.\boldsymbol{n} + \sigma\kappa\boldsymbol{n} \qquad (5)$$

$$\dot{m} h_{fg} = \dot{q} = k_v \left.\frac{\partial T}{\partial n}\right|_v - k_l \left.\frac{\partial T}{\partial n}\right|_e \qquad (6)$$

In these equations, $\boldsymbol{u}_l$ and $\boldsymbol{u}_v$ are fluid velocities in liquid and vapor phases, respectively; $\boldsymbol{u}_f$ is the velocity of the interface, and m is the vaporization rate at the interface. It is assumed that the temperature at the interface, T_f, is equal to saturation temperature at the corresponding pressure, i.e.: $T_f = T_{sat}(P_{sys})$. In general, Eqs. (1), (2), (4) and (5) should be solved for each phase and at the interface. Considering the jump condition at the interface, momentum and energy equations take the following forms:

$$\frac{\partial\rho\boldsymbol{u}}{\partial t} + \nabla.\rho\boldsymbol{u}\boldsymbol{u} = -\nabla P + \rho\boldsymbol{g} + \nabla.\mu(\nabla\boldsymbol{u} + \nabla\boldsymbol{u}^T)$$
$$+\sigma\int \delta(\boldsymbol{x} - \boldsymbol{x}_f)\kappa_f \boldsymbol{n}_f dA_f \qquad (7)$$

$$\frac{\partial\rho cT}{\partial t} + \nabla.\rho c\boldsymbol{u}T = \nabla.k\nabla T -$$
$$\left[1 - (c_v - c_l)\frac{T_{sat}}{h_{fg}}\right]\int \delta(\boldsymbol{x} - \boldsymbol{x}_f)\dot{q}_f dA_f \qquad (8)$$

Here, δ is a two- or three-dimensional delta function which is obtained by successive multiplication of single delta function. x is an arbitrary point within the solution domain, and $\boldsymbol{x}_f$ is an arbitrary point on the interface (all variables with the subscript f are related to the interface). In the past, these equations were solved using second-order projection without taking into account any phase change. If there is no phase change, then Eq. (1) reduces to $\nabla.u=0$ which characterizes incompressible flows. Here, incompressibility is applied to each phase. At the interface, however, compressibility exists due to the change in phase. Even though it is still possible to write Eq. (1) in such a way that it is compatible with the projection method, but the velocity field can be considered as follows:

$$\boldsymbol{u} = \boldsymbol{u}_v I + \boldsymbol{u}_l (1 - I) \qquad (9)$$

$$\nabla.\boldsymbol{u} = \frac{1}{h_{fg}}(\frac{1}{\rho_v} - \frac{1}{\rho_l})\int \delta(\boldsymbol{x} - \boldsymbol{x}_f)\dot{q}_f dA_f \qquad (10)$$

In general, it can be declared that the Eqs. (7), (8) and (10) should be solved. These equations are solved using a second-order temporal-spatial method on a staggered grid. I is the indicator function.

3- Results and Discussion

Fig. 1 shows the growth of the bubble at two different times. Buoyancy causes the bubble to move vertically. The upper part of the vapor bubble starts to widen while its lower part becomes thinner. However, after a certain time, due to vaporization and buoyancy force, the thickness of the vapor layer on the lower part of the cylinder becomes constant. The temperature of the cylinder wall prevents further thinning of the lower part of the bubble due to the vaporization of the liquid. The upper part of the bubble, however, continues to grow and develops a mushroom-shape. The bubble tends to be released from the vapor film, provided that the upper part continues to grow. As a result, the lower part of the bubble becomes thinner. Several factors control the release of the bubble from the vapor film. These include the cylinder temperature which rises the temperature and thereby vaporizes the liquid in the lower part of the bubbles; the growth rate of the upper part of the bubbles; also the interfacial tension which contributes to thinning of the vapor layer. Fig. 1 shows contours of the indicator function too. This function is one in liquid and zero in vapor and varies between zero and one as one moves across the interface. The higher the grid resolution, the lower is the thickness of this zone (the zone where the indicator function changes.) However, considering the fact that the solid body is introduced into the flow using its specific indicator function, the cylinder boundary is not evident in this figure.
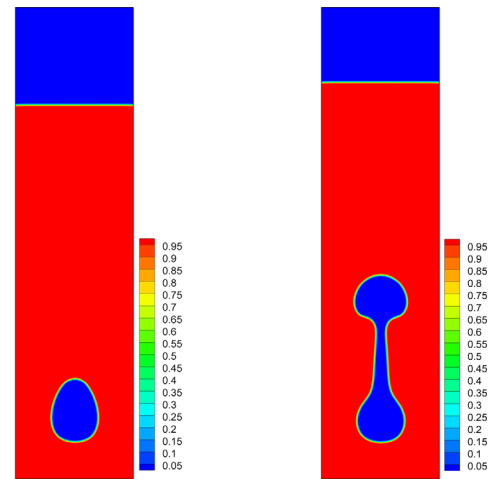
Fig. 2. Contours of the indicator function at 5s (left) and 15s (right)

Fig. 2 demonstrates the growth and rise of bubbles at different times for 4 rows of cylinders. As can be seen, the vapor bubbles grow from the lower cylinders and once passed through the upper cylinders, surround them. Furthermore, the grown bubbles further rise towards the vapor layer on top of the computational domain.
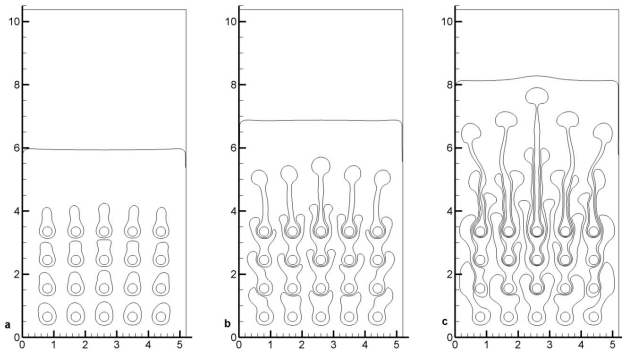
Fig. 2. The shape of the interface at 5, 10, 15s

4- Conclusions

Film boiling was studied on the two-cylinder arrangement. The effect of the cylinder spacing on the Nusselt number for the upper cylinder was considered. It is observed that the cylinder spacing has a weak effect on the Nusselt number. The effect of the orientation angle between the two cylinders on the Nusselt number was studied next. The Nusselt number is strongly dependent on the relative orientation angle. It becomes maximum at an orientation angle 90°. The effect of diameter of the lower cylinder on the Nusselt number of the upper cylinder was also investigated. The overall result was that the larger the level of flow disturbance, the higher will be the Nusselt number. The level of disturbance is indeed a function of the engagement of vapor bubbles generated from the lower cylinder with the upper cylinder. As a result, a larger cylinder imposes larger disturbances which in turns enhance the Nusselt number on the upper cylinder. The number of cylinders was increased in order to investigate the effect of the adjacent cylinders on the overall Nusselt number. Two arrangements (regular and staggered) were considered, and the cylinders were arranged in different numbers of rows. The effect of the number of rows on the Nusselt number of the cylinders in the upper row was investigated for every arrangement, and a comparison was made between the two arrangements. It was found that the Nusselt numbers on the upper cylinders are more non-uniform in the staggered arrangement compared to the regular arrangement. Also, the overall Nusselt number was higher for the upper row in staggered arrangement compared to the regular arrangement. In fact, the results of this section can be used for design, manufacturing and optimization of the heat exchangers wherein the film boiling regime exist.

References

[1] A. Swain, M.K. Das, A review on saturated boiling of liquids on tube bundles, *Heat and Mass Transfer*, 50(5) (2014) 617-637.

[2] M.-G. Kang, Local pool boiling coefficients on horizontal tubes, *Journal of mechanical science and technology*, 19(3) (2005) 860-869.

[3] A. Esmaeeli, G. Tryggvason, Computations of film boiling. Part I: numerical method, *International journal of heat and mass transfer*, 47(25) (2004) 5451-5461.